

Nonstationary Laguerre-Gaussian states vs Landau ones: choose your fighter

G.K. Sizykh,^{*} A.D. Chaikovskaia, D.V. Grosman, I.I. Pavlov, and D.V. Karlovets[†]
School of Physics and Engineering, ITMO University, 197101 St. Petersburg, Russia

Although the widely used stationary Landau states describe electrons with a definite orbital angular momentum (OAM) in a magnetic field, it is the lesser known nonstationary Laguerre-Gaussian (NSLG) states that appropriately characterize vortex electrons after their transfer from free space to the field. The reason is boundary conditions lead to oscillations of the r.m.s. radius (the transverse coherence length) of the electron packet that has entered a solenoid. We comprehensively investigate properties of the NSLG states and establish their connections with the Landau states. For instance, we show that the transverse coherence length of an electron in the field usually oscillates around a value greatly exceeding the Landau state coherence length. We also discuss sensitivity of the NSLG states to a small misalignment between the propagation axis of a free electron and the field direction, which is inevitable in a real experiment. It is shown that for any state-of-the-art parameters, the corrections to the observables are negligible, and the electron OAM stays robust to a small tilt of the propagation axis. Finally, we draw analogies between a quantum wave packet and a classical beam of many particles in phase space, calculating the mean emittance of the NSLG states, which acts as a measure of their quantum nature.

I. INTRODUCTION

During the last two decades, electrons with orbital angular momentum (OAM), also known as twisted or vortex electrons, have successfully transitioned from theoretical concept [1–12] to experimental realizations [13–18] and practical implementations [13, 19–21]. Nevertheless, this is still a relatively new area in quantum microscopy and particle physics [22]. In particular, generation and lensing of twisted electrons should be thoroughly investigated so they could become a reliable and useful tool in atomic and particle physics, studies of magnetic properties of materials [19, 20], and other associated fields.

There are two common approaches to obtain twisted electrons: using phase plates [23–25] and computer-generated holograms [13, 14, 26, 27]. In free space such electrons are modelled by either Bessel beams [2, 3, 5, 7, 9] or Laguerre-Gaussian states [6, 10]. Whereas the former possess a definite energy, they cannot appropriately characterize real-life electron states, as Bessel beams are non-normalizable. Laguerre-Gaussian states, on the contrary, are normalizable non-stationary wave packets with an energy spread.

Regardless of the generation method, control over the twisted beams transfer through magnetic lenses is crucial for their further use as a diagnostic tool or in other applications. There have already been attempts to investigate the propagation of electrons carrying OAM in magnetic fields [3, 4, 28–31]. Nonetheless, for practical applications, the transfer of a vortex electron across a boundary between free space and a solenoid (in a setup similar to that of Fig. 1) should be taken into account. The boundary conditions are defined by the state of the electron entering the magnetic field from free space or

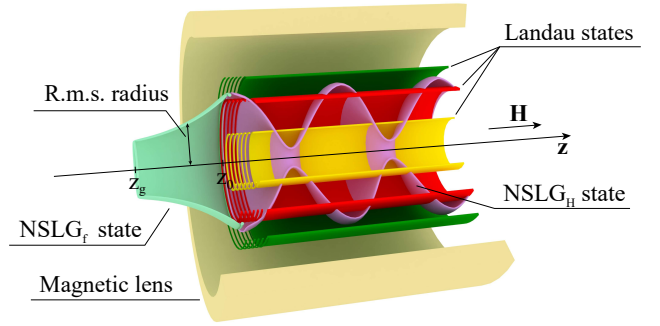


Figure 1: Transfer of a free Laguerre-Gaussian electron through a magnetic lens. z_g and z_0 are the positions of the electron source and the boundary, respectively.

generated in the field, for example, with a magnetized cathode [29]. These conditions crucially affect further propagation of the electron inside the magnetic lens.

Commonly, an electron in a magnetic field is presumed to be in a stationary Landau state [29, 32, 33]. However, it seems highly unlikely that an electron evolves to the Landau state right after crossing the boundary in an infinitesimal period of time. Therefore, the common approach with the Landau states employed, e.g., in [29, 33], seems to have limited applicability. Moreover, we can set the problem of an electron in a constant and homogeneous magnetic field using one of the two distinct gauges for the vector potential \mathbf{A} , both leading to the same field $\mathbf{H} = \{0, 0, H\}$ [34], but to different sets of solutions: namely, Hermite-Gaussian and Laguerre-Gaussian beams. Clearly, these are two distinct physical states with different quantum numbers, and it is the boundary (or initial) conditions that determine the choice of the gauge and of the electron quantum state. Here we argue that, generally, it is *nonstationary Laguerre-Gaussian* (NSLG) states rather than the Landau ones that correctly describe the transition process with ap-

^{*} georgii.sizykh@metalab.ifmo.ru

[†] dmitry.karlovets@metalab.ifmo.ru

appropriate boundary conditions. Introducing a boundary makes the root-mean-square (r.m.s) radius of the electron oscillate around a value significantly larger than that predicted by the stationary Landau states.

The aim of this paper is to elaborate on the nonstationary dynamics of electrons in a magnetic field and to investigate the NSLG states in detail. In Sec. II, we introduce these states and provide their comprehensive description both in free space and in a magnetic field. We focus on the electron transverse dynamics, as the longitudinal one is not affected by the magnetic field. The transverse dynamics is supposed to be nonrelativistic and the restrictions imposed are discussed in Sec. III. In Sec. IV, we show that in the limit of $H \rightarrow 0$ the NSLG states inside the solenoid turn into free-space Laguerre-Gaussian wave packets. Further, we consider a mismatch between a free NSLG electron propagation axis and the magnetic field direction. In Sec. V, the NSLG and the Landau states are compared, particularly, their sizes. Then we decompose the former into the superposition of the latter. Finally, in Sec. VI, analogies are drawn between a classical particle beam and a quantum wave packet. We introduce a quantum r.m.s. emittance and apply it to the NSLG states.

Electron spin has no qualitative impact on our results and is neglected. Throughout the paper, natural system of units $\hbar = c = 1$ is used. The electron charge is $e = -e_0$, where $e_0 > 0$ is the elementary charge. Alongside with the electron mass, we use the Compton wavelength $\lambda_C = m^{-1}$.

II. NSLG STATES

A. Longitudinal and transverse dynamics

In nonrelativistic quantum mechanics, electron dynamics is described by the Schrödinger equation

$$i \frac{\partial \Psi(\mathbf{r}, t)}{\partial t} = \hat{\mathcal{H}} \Psi(\mathbf{r}, t). \quad (1)$$

Both in vacuum and inside a magnetic lens, we can single out the motion along the field and factorize the solution of Eq. (1) as $\Psi(\mathbf{r}, t) = \Psi_{\perp}(\rho, \varphi, t) \Psi_{\parallel}(z, t)$.

The longitudinal wave function is assumed to be a wave-packet solution to the one-dimensional Schrödinger equation

$$i \frac{\partial \Psi_{\parallel}}{\partial t} = \frac{\hat{p}_z^2}{2m} \Psi_{\parallel} \quad (2)$$

with a nonzero average z -projection of the velocity operator $-i\lambda_C \langle \partial_z \rangle = v$. Generally, it can be presented as a superposition of plane waves with different momenta:

$$\Psi_{\parallel}(z, t) = \int_{-\infty}^{\infty} g(p_z) \exp\left(ip_z z - i \frac{p_z^2}{2m} t\right) \frac{dp_z}{2\pi}. \quad (3)$$

Its explicit form does not affect the transverse dynamics. From here on, we only discuss the transverse dynamics of twisted electrons and omit the “ \perp ” sign to simplify the notation.

B. General NSLG states

In the present work, we are interested in the transverse dynamics of an electron after it crosses the boundary between vacuum and a magnetic field area. In both regions, the electron can be described by the following wave function:

$$\Psi_{nl}(\boldsymbol{\rho}, t) = N_{nl} \frac{\rho^{|l|}}{\sigma^{|l|+1}(t)} L_n^{|l|} \left(\frac{\rho^2}{\sigma^2(t)} \right) \times \exp \left[il\varphi - i\Phi_G(t) - \frac{\rho^2}{2\sigma^2(t)} \left(1 - i \frac{\sigma^2(t)}{\lambda_C R(t)} \right) \right], \quad (4)$$

which we call a *nonstationary Laguerre-Gaussian* state. Here, $L_n^{|l|}$ are generalized Laguerre polynomials, $n = 0, 1, 2, \dots$ is the radial quantum number, and $l = 0, \pm 1, \pm 2, \dots$ is the OAM, which is conserved in axially symmetric fields even with weak inhomogeneities [29]. The difference between NSLG states in free space (NSLG_f) and in the magnetic field (NSLG_H) is determined by optical functions: dispersion $\sigma(t)$, radius of curvature $R(t)$, and Gouy phase $\Phi_G(t)$. The normalization constant in Eq. (4) is defined by the standard condition of a single particle in the volume:

$$N_{nl} = \sqrt{\frac{1}{\pi} \frac{n!}{(n + |l|)!}}. \quad (5)$$

The NSLG states were briefly introduced in our recent work [35] as means to account for the boundary crossing that provide consistent description of the electron state in regions with and without magnetic field. Here we dwell deeper into the dynamics of these states and discuss their properties from different angles.

The state with the transverse part (4) corresponds to an electron moving rectilinearly along the z -axis, which means that

$$\langle \boldsymbol{\rho} \rangle = 0, \quad \langle \hat{\mathbf{v}} \rangle = 0, \quad (6)$$

where $\hat{\mathbf{v}} = -i\nabla_{\perp}/m - e\mathbf{A}/m$. The r.m.s. radius of the NSLG state is proportional to the dispersion:

$$\rho(t) \equiv \sqrt{\langle \rho^2 \rangle - \langle \boldsymbol{\rho} \rangle^2} = \sigma(t) \sqrt{2n + |l| + 1}. \quad (7)$$

We can directly check that states (4) form an orthonormal set:

$$\int \Psi_{n'l'}^*(\boldsymbol{\rho}, t) \Psi_{nl}(\boldsymbol{\rho}, t) d^2\rho = \delta_{nn'} \delta_{ll'}. \quad (8)$$

The set is also complete (see the proof in the Appendix A).

C. NSLG states in free space

In this section, we derive the optical functions of the NSLG_f states, which will later determine the initial conditions for the states in the field.

In free space, the transverse Hamiltonian is

$$\hat{\mathcal{H}}_f = \frac{\hat{\mathbf{p}}_{\perp}^2}{2m}, \quad (9)$$

where the index “f” stands for “free”. To derive the optical functions and then the NSLG_f state, the wave function (4) can be substituted into the Schrödinger equation (1) with the Hamiltonian (9). This leads to the system of equations

$$\begin{aligned} \frac{1}{R(t)} &= \frac{\sigma'(t)}{\sigma(t)}, \\ \frac{1}{\lambda_C^2 R^2(t)} + \frac{1}{\lambda_C^2} \left[\frac{1}{R(t)} \right]' &= \frac{1}{\sigma^4(t)}, \\ \frac{1}{\lambda_C} \Phi'_G(t) &= \frac{2n + |l| + 1}{\sigma^2(t)}, \end{aligned} \quad (10)$$

where the primes stand for time derivatives. Instead of $R(t)$, we prefer using the dispersion divergence rate $\sigma'(t) = \sigma(t)/R(t)$ alongside with $\sigma(t)$ and $\Phi(t)$ to characterize the NSLG states.

To find the unique solution of the system (10), the initial conditions should be specified. In real experiment, twisted electrons are generated at the beam waist:

$$\sigma_f(t_g) = \sigma_w, \quad \sigma'_f(t_g) = 0, \quad \Phi_f(t_g) = 0, \quad (11)$$

where t_g is the time when the twisted electron is generated and σ_w is the dispersion at the waist. We set $\Phi_f(t_g) = 0$, because a constant phase factor does not change the state.

The optical functions $\sigma_f(t)$ and $\Phi_f(t)$ satisfying the system (10) with the initial conditions (11) are

$$\sigma_f(t) = \sigma_w \sqrt{1 + \frac{(t - t_g)^2}{\tau_d^2}}, \quad (12)$$

$$\Phi_f(t) = (2n + |l| + 1) \arctan \left(\frac{t - t_g}{\tau_d} \right).$$

Here, $\tau_d = \sigma_w^2/\lambda_C$ is the diffraction time. The NSLG states (4) with $\sigma(t)$ and $\Phi_G(t)$ given by Eqs. (12) and $R(t) = \sigma_f(t)/\sigma'_f(t)$ are the nonstationary counterparts [29, 36, 37] of the well-known paraxial *free Laguerre-Gaussian* wave packets [3, 14, 15, 18, 22].

According to Eqs. (12) and (7), the r.m.s. radius of the NSLG_f state is

$$\rho_f(t) = \rho_w \sqrt{1 + \frac{(t - t_g)^2}{\tau_d^2}} \quad (13)$$

where $\rho_w = \sigma_w \sqrt{2n + |l| + 1}$. This expression illustrates quadratic divergence of the r.m.s. radius near the beam waist and linear growth far from it.

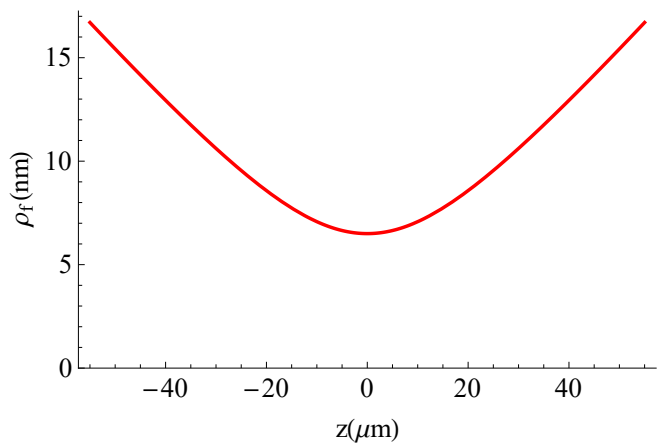


Figure 2: NSLG_f packet r.m.s. radius based on the parameters from the experiment [15]. Electron energy $E_{\parallel} = 300$ KeV (corresponding velocity $v \approx 0.78c$), $n = 0$, $l = 3$, and $\sigma_g = 3.25$ nm (corresponding $\tau_d = 9 \times 10^{-5}$ ns).

Since the NSLG states do not generally possess definite energy, we consider its expectation value. For the NSLG_f state given by Eqs. (4) and (12), taking into account $R(t) = \sigma(t)/\sigma'(t)$,

$$\langle E \rangle_f = \frac{2n + |l| + 1}{2\lambda_C} \left(\frac{\lambda_C^2}{\sigma_f^2(t)} + \sigma_f'^2(t) \right). \quad (14)$$

The first term in Eq. (14) stems from the size effect and decreases with the volume occupied by the wave packet. The second term has a kinetic nature and is responsible for the radial divergence of the state. The free Hamiltonian (9) does not depend on time, which means that the average energy is constant. Indeed, by substituting the dispersion (12) and its derivative into Eq. (14), we obtain

$$\langle E \rangle_f = \frac{2n + |l| + 1}{2\tau_d}. \quad (15)$$

We illustrate the dynamics of the NSLG_f wave packet obtained in the experiment of Guzzinati et al. [15] (see Figs. 3, 4 there) in Fig. 2. The electron has the following parameters: electron energy $E_{\parallel} = 300$ KeV (and the corresponding velocity $v \approx 0.78c$), $n = 0$, $l = 3$ (in [15] l is designated as m), beam waist dispersion $\sigma_w = 3.25$ nm (corresponding r.m.s. radius of the waist $\rho_w = \sqrt{2n + |l| + 1} = 6.5$ nm), and diffraction time $\tau_d = 9 \times 10^{-5}$ ns.

Note that we plot the beam radius, while in the work [15] (see Fig. 4(a) there), the beam diameter is depicted. Guzzinati et al. observed several rings as they blocked half of the initial NSLG_f beam and obtained a superposition of the NSLG_f states. However, in this case, the original NSLG_f state makes the dominant contribution, which allows us to reproduce their results.

D. Landau states

Let us now turn to a twisted electron state inside a solenoid. We describe the solenoid as a semi-infinite stationary and homogeneous magnetic field $\mathbf{H} = H\theta(z - z_0)\mathbf{e}_z$, $\mathbf{e}_z = (0, 0, 1)$. The step function $\theta(z)$ reflects the hard-edge boundary located at z_0 . We assume the longitudinal part of the wave function to be narrow enough, so that the field can be considered to be suddenly switched on at the time t_0 .

Before moving to the NSLG_H states, we would like to briefly remind the reader of the Landau ones. They are stationary solutions to the Schrödinger equation (1) with the transverse Hamiltonian

$$\hat{\mathcal{H}} = \frac{(\hat{\mathbf{p}}_{\perp} - e\mathbf{A})^2}{2m}. \quad (16)$$

Recall the aforementioned gauge issue: in the original work of Landau, the vector potential is chosen as [38]

$$\mathbf{A} = -Hy\mathbf{e}_x. \quad (17)$$

The Landau states that are the solutions of the Schrödinger equation (1) with the Hamiltonian (16) defined by the vector potential in the Landau gauge (17) are given by Hermite-Gaussian functions

$$\begin{aligned} \Psi(x, y, z, t) \propto H_s \left(\frac{y - \tilde{\sigma}_L^2 p_x}{\tilde{\sigma}_L} \right) \exp \left(-\frac{(y - \tilde{\sigma}_L^2 p_x)^2}{2\tilde{\sigma}_L^2} \right) \times \\ \exp \left(ip_x x + ip_z z - i\frac{\omega}{2}(2s + 1)t \right), \end{aligned} \quad (18)$$

where $\tilde{\sigma}_L = \sqrt{1/|eH|}$, $\omega = |eH|/m$ is the cyclotron frequency, and $s = 0, 1, 2, \dots$ is the principal quantum number.

Alternatively, one can choose the symmetric gauge for the vector potential:

$$\mathbf{A} = \frac{H}{2}\rho\mathbf{e}_{\varphi}. \quad (19)$$

where $\mathbf{e}_{\varphi} = \mathbf{e}_y \cos \varphi - \mathbf{e}_x \sin \varphi$ is the azimuthal unit vector. Such a choice preserves the axial symmetry of the problem, and the corresponding solutions of the Schrödinger equation have definite values of the OAM (see, e.g., [39]):

$$\begin{aligned} \Psi_{nl}^{(L)}(\rho, \varphi, t) = N_{nl} \left(\frac{\rho^{|l|}}{\sigma_L^{|l|+1}} \right) L_n^{|l|} \left[\frac{\rho^2}{\sigma_L^2} \right] \times \\ \exp \left[-\frac{\rho^2}{2\sigma_L^2} + il\varphi - iE_L t \right], \end{aligned} \quad (20)$$

where $\sigma_L = \sqrt{2/|eH|}$ is the r.m.s. radius of the Landau state with $n = l = 0$. The normalization constant N_{nl} in Eq. (20) is given by Eq. (5). In what follows, by Landau states, we mean the wave function (20) and not (18), which can be viewed as yet another initial condition.

The energy E_L of the Landau states is

$$E_L = \frac{\omega}{2}(2n + |l| + l + 1) = \frac{\omega}{2}(2n + |l| + 1) + l\mu_B H, \quad (21)$$

where $\mu_B = |e|/(2m)$ is the Bohr magneton. The last term in Eq. (21) is the energy of the magnetic moment $-l\mu_B$ in the field H . Note that the electron energy in a Landau state is infinitely degenerate for $l \leq 0$ due to the exact compensation of kinetic and magnetic ‘‘orbital motions’’. However, for $l > 0$, the two terms add up and double the contribution to the energy.

The r.m.s. radius of the Landau states (20) is constant and equal to

$$\rho_L = \sigma_L \sqrt{2n + |l| + 1}. \quad (22)$$

Note that in a given magnetic field, there is only a countable set of possible r.m.s. radii of an electron described by the Landau states. In reality, an electron enters the field from free space or is generated in the field with an arbitrary size that must evolve continuously. If this size does not fall within the countable set of possible r.m.s. radii, the free electron cannot find a suitable Landau state to transform into. Moreover, even if the r.m.s. radius of the electron equals that of the Landau state, the divergence rate must also vanish. Thus, taking into account the initial conditions, we are generally led to a non-stationary electron state in the field, which is properly described by the NSLG_H state.

E. NSLG states in the field

Similarly to the NSLG_f, one can derive the NSLG_H states in the magnetic field. Substituting the state (4) into the Schrödinger equation (1) with the Hamiltonian (16) we obtain

$$\begin{aligned} \frac{1}{R(t)} &= \frac{\sigma'(t)}{\sigma(t)}, \\ \frac{1}{\lambda_C^2 R^2(t)} + \frac{1}{\lambda_C^2} \left[\frac{1}{R(t)} \right]' &= \frac{1}{\sigma^4(t)} - \frac{1}{\sigma_L^4}, \\ \frac{1}{\lambda_C} \Phi_G'(t) &= \frac{l}{\sigma_L^2} + \frac{2n + |l| + 1}{\sigma^2(t)}. \end{aligned} \quad (23)$$

This system is very similar to the set of equations for the optical functions of a free electron state (10), yet it results in a drastically different dynamics.

Although one can take arbitrary initial conditions to specify the unique solution of the system (23), in a real experiment, they are determined by the incoming electron state. This prompts us to use the values of the dispersion, its time derivative, and the Gouy phase of the NSLG_f electron at the time t_0 when it enters the solenoid as the initial conditions for the NSLG_H state:

$$\begin{aligned} \sigma(t_0) &= \sigma_f(t_0) = \sigma_0, \\ \sigma'(t_0) &= \sigma_f'(t_0) = \sigma'_0, \\ \Phi_G(t_0) &= \Phi_f(t_0) = \Phi_0. \end{aligned} \quad (24)$$

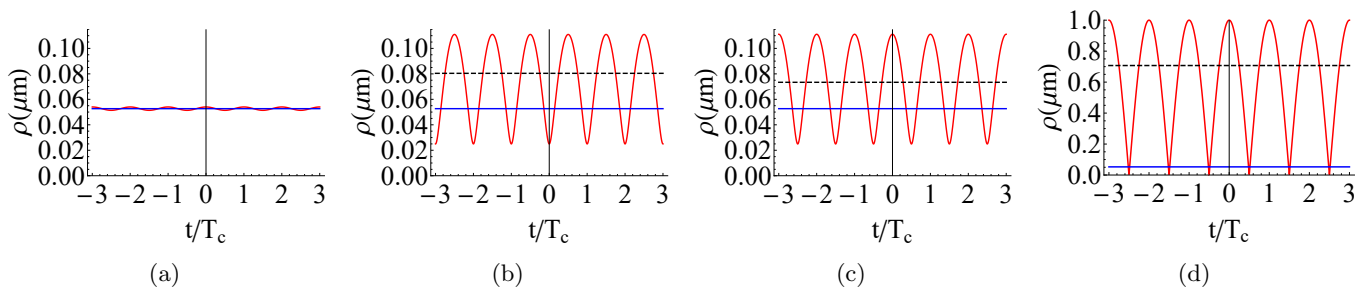


Figure 3: The NSLG_H packet r.m.s. radii (in red) for different ρ_0 ; $\rho_L \approx 52.7$ nm is in blue. Black dashed lines correspond to ρ_{st} given by Eq. (28). In each subfigure $H = 1.9$ T ($T_c \approx 0.02$ ns.), $n = 0$, $l = 3$, $\rho'_0 = 0$.
(a) $\rho_0 = 54$ nm, (b) $\rho_0 = 25$ nm, (c) $\rho_0 = 111.1$ nm, (d) $\rho_0 = 1\mu\text{m}$.

Following the seminal approach of Silenko et al. [28], we derive the dispersion of the NSLG_H electron from Eqs. (23) with the initial conditions (24):

$$\begin{aligned} \sigma(t) &= \sigma_{st} \sqrt{1 + \sqrt{1 - \left(\frac{\sigma_L}{\sigma_{st}}\right)^4} \sin[s(\sigma_0, \sigma'_0)\omega(t - t_0) - \theta]}, \\ \sigma_{st}^2 &= \frac{\sigma_0^2}{2} \left(1 + \left(\frac{\sigma_L}{\sigma_0}\right)^4 + \left(\frac{\sigma'_0 \sigma_L^2}{\lambda_C \sigma_0}\right)^2\right), \\ \theta &= \arcsin \frac{1 - (\sigma_0/\sigma_{st})^2}{\sqrt{1 - (\sigma_L/\sigma_{st})^4}}, \end{aligned} \quad (25)$$

where the sign function is

$$s(\sigma_0, \sigma'_0) = \begin{cases} \text{sgn}(\sigma'_0), & \sigma'_0 \neq 0, \\ \text{sgn}(\sigma_L - \sigma_0), & \sigma'_0 = 0, \\ 0, & \sigma_0 = \sigma_L \text{ and } \sigma'_0 = 0. \end{cases} \quad (26)$$

This dispersion describes the oscillations of the r.m.s. radius of the electron inside the solenoid with a period $T_c = 2\pi/\omega$. The value θ is the initial phase of the oscillations.

We should also note that states similar to those discussed in this section are presented in the books [40, 41] as coherent states of an electron in the magnetic field with the vector potential (19). Another approach to obtaining the NSLG_H wave functions using quantum Arnold transformation was recently realized in [42].

The parameter σ_{st}^2 is the period-averaged dispersion square

$$\sigma_{st}^2 = \frac{1}{T_c} \int_0^{T_c} \sigma^2(t) dt \geq \sigma_L^2. \quad (27)$$

We further use the corresponding time-averaged radius square

$$\rho_{st}^2 = (2n + |l| + 1)\sigma_{st}^2 \geq \rho_L^2 \quad (28)$$

as a characteristic size of the oscillating wave packet. The inequalities in Eqs. (27), (28) are derived and discussed in Sec. VB.

The oscillations of the r.m.s. radius of the NSLG_H states are shown in Fig. (3). We consider the magnetic field $H = 1.9$ T, typical for transmission electron microscopes, and quantum numbers $n = 0$, $l = 3$ (the corresponding $\rho_L \approx 52.7$ nm) [17]. For simplicity, we set $\rho'_0 = 0$. A nonzero initial value of the divergence rate ρ'_0 alters the initial phase of the oscillations θ and the amplitude in accordance with Eqs. (25), but the picture remains qualitatively the same. We discuss how nonzero divergence rate affects the r.m.s. radius oscillations in the Appendix B.

Now let us discuss the possible oscillation regimes. In Fig. 3a, the free electron size at the boundary $\rho_0 = 54$ nm is close to ρ_L . The r.m.s. radius of the corresponding NSLG_H state oscillates around approximately the same value with a negligibly small amplitude. As we will discuss later (see Sec. VC), such an electron can be considered to be in a Landau state to a good extent. In Fig. 3b, $\rho_0 = 25$ nm is significantly smaller than ρ_L . In this case, the magnetic field "tries" to stretch the wave packet to the size of the corresponding Landau state. By the time it happens, the r.m.s. radius of the NSLG_H state acquires a nonzero divergence rate and continues broadening past ρ_L . In Fig. 3c, $\rho_0 = 111.1$ nm is larger than ρ_L , and their ratio is exactly the inverse of that in 3b. Here, in contrast, the field "tries" to shrink the packet at first; as a result, the r.m.s. radius decreases past the Landau state value and oscillates. Note that for two states with initial sizes $\rho_{0,1}$ and $\rho_{0,2}$, if $\rho_{0,1}/\rho_L = \rho_L/\rho_{0,2}$, the oscillations only differ by a π phase shift and are otherwise identical. Finally, in Fig. 3d, we consider an electron of the size $\rho_0 = 1\mu\text{m}$ much larger than ρ_L . Then, the oscillations of the r.m.s. radius of the NSLG_H electron "experience" sharp bounces from their lowest value. Similar behavior (shifted by half a period) is observed when the initial NSLG_H packet size is much less than the Landau radius.

Thus, from Fig. 3, we can identify three oscillation regimes:

1. Landau-like regime: the r.m.s. radius of the NSLG_H state is almost constant,
2. Sine-like regime: the stationary r.m.s. radius (28)

is always larger than the Landau radius, but they have the same order of magnitude,

3. Bouncing regime: the r.m.s. radius of the NSLG_H state is sharply “bouncing off” the minimal value, and its time-averaged value is much larger than that of the Landau state.

The oscillating behavior of the NSLG_H states’ r.m.s. radius reminds that of optical Gaussian beams in ducts

or graded-index optical waveguides [43]. A duct analogue of σ_L^{-2} is $\sigma_O^{-2} = \lambda/(\pi\sqrt{n_2})$, where λ is the beam wavelength in a medium and $n_2 = d^2n(\rho)/d\rho^2|_{\rho=0}$ is the second derivative of the refractive index with respect to the radial coordinate near the symmetry axis. Now let us consider an optical Gaussian beam with a waist dispersion distinct from σ_O . In this case, the r.m.s. radius of such a beam will oscillate similar to the r.m.s. radius of the NSLG_H state, whose oscillations are shown in Fig. 3.

The Gouy phase of the NSLG_H state is

$$\Phi_G(t) = \Phi_0 + \frac{l\omega(t-t_0)}{2} + (2n+|l|+1)s(\sigma_0, \sigma'_0) \times \left[\arctan \left(\frac{\sigma_{st}^2}{\sigma_L^2} \tan \frac{s(\sigma_0, \sigma'_0)\omega(t-t_0) + \theta}{2} + \frac{\sigma_{st}^2}{\sigma_L^2} \sqrt{1 - \left(\frac{\sigma_L}{\sigma_{st}}\right)^4} \right) - \arctan \left(\frac{\sigma_{st}^2}{\sigma_L^2} \tan \frac{\theta}{2} + \frac{\sigma_{st}^2}{\sigma_L^2} \sqrt{1 - \left(\frac{\sigma_L}{\sigma_{st}}\right)^4} \right) \right]. \quad (29)$$

In Eq. (29), the arc tangent should be treated as a multi-valued function for the Gouy phase to be continuous. The Gouy phase for $H = 1.9$ T ($\rho_L \approx 64$ nm), $\rho_0 \approx 122$ nm, $\rho'_0 = 0$, and $\Phi_0 = 0$ is shown in Fig. 4. The red, blue, and green lines correspond to three different pairs of quantum numbers $(n, l) = \{(0, 0), (0, 1), (1, 1)\}$, respectively.

A free Gaussian beam gains a phase factor of π while travelling from distant past to distant future [3, 15, 18, 22, 28, 43, 44]. Most of the phase gain is accumulated around the waist of the packet. A free Laguerre-Gaussian beam acquires a phase factor of $(2n + |l| + 1)\pi$ the same way, propagating near its waist. Inside the field, the dynamics are periodic, and the electron state acquires this phase factor each cyclotron period. Moreover, interaction of the OAM with the field provides an additional Zeeman-type phase $l\pi$ [3, 15]. Thus, the phase accumulated by the NSLG_H state per T_c is $(2n + |l| + l + 1)\pi$.

The average energy of the NSLG_H electron is

$$\langle E \rangle = \frac{\omega}{2}(2n + |l| + 1) \frac{\sigma_{st}^2}{\sigma_L^2} + l\mu_B H. \quad (30)$$

Generally, when $\sigma_{st}^2/\sigma_L^2 > 1$, the kinetic rotation prevails over the magnetic one. Moreover, for OAM directed opposite to the field, the two terms do not compensate each other, which removes the degeneracy of energy levels compared to the Landau states. Note that the average energy of the NSLG_H state (30) is always larger than that of the Landau one (21), and they are equal only for $\sigma_{st} = \sigma_L$, when the two states coincide (see Sec. V).

Although the NSLG_H states have not yet been observed directly, an indirect evidence for their existence could have been obtained in the experiment of Schattschneider et al. [17]. In this experiment, the authors observed a possible part of the oscillations inherent to the NSLG_H states (see Fig. 2b in [17]). In Fig. 5, we reproduce the evolution of the electron r.m.s. radius with the parameters from this work: electron energy

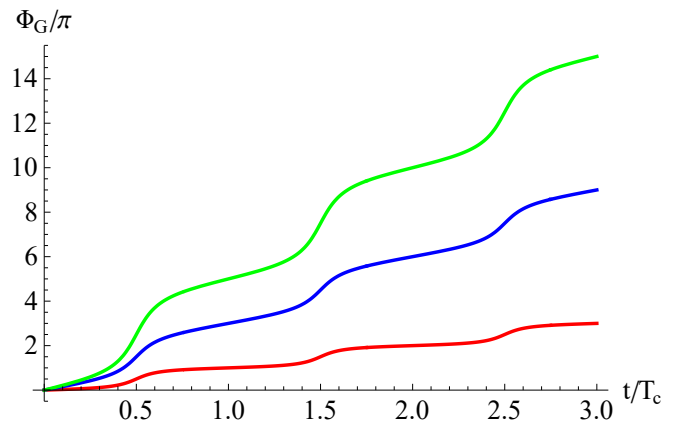


Figure 4: Gouy phase $\Phi_G(t)$ of the NSLG_H wave packet. The field strength $H = 1.9$ T (corresponding $\rho_L \approx 37$ nm), $\rho_0 \approx 71$ nm, $\rho'_0 = 0$, $T_c \approx 0.02$ ns, and $\Phi_0 = 0$. The quantum numbers are: $n = 0, l = 0$ (red line); $n = 0, l = 1$ (blue); and $n = 1, l = 1$ (green).

$E_{\parallel} = 200$ KeV (corresponding velocity $v \approx 0.7c$), $n = 0, l = 1$ (in the work, l is designated as m), $\rho_0 \approx 67.5$ nm, $\rho'_0 \approx -4.4 \times 10^{-4}$, and $H = 1.9$ T. The black vertical line in Fig. 5 cuts off the z -region observed in the experiment. We extend this region a little to show the reader the subsequent bounce of the r.m.s. radius. Thus, we put forward the idea that the authors might have dealt with the NSLG_H state.

III. TRANSVERSELY RELATIVISTIC WAVE PACKETS

We assume $E \ll mc^2$ while investigating twisted electrons in this work, but Eqs. (14), (21), and (30) make it clear that this condition is no longer valid for large n and

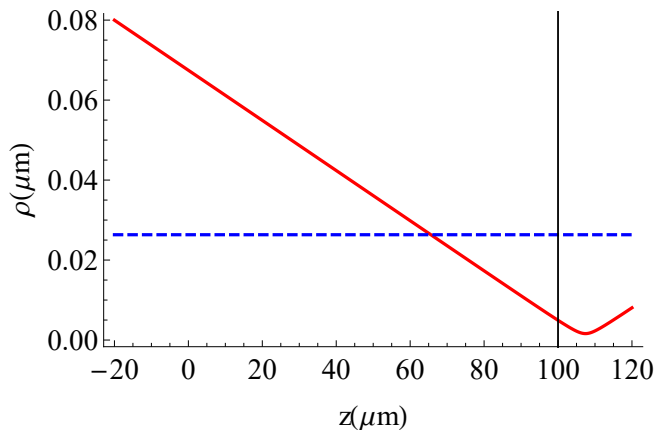


Figure 5: NSLG_H packet r.m.s. radius (in red) and Landau dispersion (in blue) based on the experiment [17]. We plot σ_L and not ρ_L to reproduce the Fig. 2b from [17]. A black vertical line marks the maximal value of z in the work [17]. Longitudinal energy $E_{\parallel} = 200$ KeV (corresponding velocity $v \approx 0.7c$), $n = 0, l = 1, \rho_0 \approx 67.5$ nm, $\rho'_0 \approx -4.4 \times 10^{-4}$, and $H = 1.9$ T (corresponding $\sigma_L \approx 26$ nm).

$|l|$. Although in modern experiments, $n \sim 1$, beams with OAM values of several hundred [45] and even thousand \hbar [46, 47] have already been generated. The restriction $E \ll mc^2$ sets the validity limits of our calculations and gives estimates of the quantum numbers that require relativistic treatment of the transverse dynamics. Furthermore, it allows considering beams that are transversely relativistic and longitudinally nonrelativistic, in contrast to those produced in accelerators nowadays.

Let us now estimate the quantum numbers n and l such that $\langle E \rangle \sim mc^2$. We start with an NSLG_f electron with energy $\langle E \rangle$ given by Eq. (15). Using $\tau_d = \rho_w^2 / [(2n + |l| + 1)\lambda_C]$, we obtain a restriction on the quantum numbers of the free electron:

$$2n + |l| + 1 \ll \frac{\rho_w}{\lambda_C}. \quad (31)$$

Typically, twisted electrons are generated with $\rho_w \sim 1$ μm . For such particles, the value in the r.h.s. of Eq. (31) is of the order of 10^6 . However, being refocused to a 1 nm waist size, electrons with quantum numbers of the order of 10^3 become transversely relativistic. Such focusing is easily achievable with appropriate magnetic lenses [17]. Thus, transversely relativistic free twisted electrons can be obtained in experiment already.

Applying the condition $\langle E \rangle \ll mc^2$ for a Landau state, we get

$$\sqrt{(2n + |l| + l + 1)} \ll \frac{\sigma_L}{\lambda_C}. \quad (32)$$

Note that in free space, we fix the r.m.s. radius of the generated electron ρ_w , but in a magnetic field, it is the

dispersion σ_L that is defined by the field strength. For example, if the field strength is of the order of 1 T, $\sigma_L \sim 36$ nm, and the r.h.s. of the inequality (32) is of the order of 10^5 . For negative values of l , the l.h.s. of Eq. (32) does not depend on OAM at all. Therefore, when the magnetic and the kinetic rotations of the Landau state compensate each other, such a state remains nonrelativistic for any attainable values of n and $|l|$. However, for $l > 0$, the relativistic regime cannot be achieved either, as it would require OAM of the order of 10^{10} .

For the NSLG_H states, the relativistic regime is more feasible than for the Landau counterparts, because NSLG_H kinetic energy is enhanced by the factor σ_{st}^2/σ_L^2 . Indeed, for an NSLG_H wave packet, we obtain

$$\sqrt{\left[(2n + |l| + 1) \frac{\sigma_{st}^2}{\sigma_L^2} + l \right]} \ll \frac{\sigma_L}{\lambda_C}. \quad (33)$$

Usually, the factor $\sigma_{st}^2/\sigma_L^2 \gg 1$; for example, in the work [17], $\sigma_{st}^2/\sigma_L^2 \approx 31$. This allows us to simplify the above condition:

$$\sqrt{(2n + |l| + 1)} \ll \frac{\sigma_L}{\lambda_C} \frac{\sigma_L}{\sigma_{st}}. \quad (34)$$

The additional factor σ_L/σ_{st} in the r.h.s. of this inequality eases the requirements on the quantum numbers to obtain transversely relativistic states. For instance, in the experiment of Schattschneider and colleagues [17], the r.h.s. of Eq. (34) is of the order of 10^4 . This value can be reduced even more, for example, by increasing ρ_0 . To increase ρ_0 , one can simply move the solenoid further from the source of twisted electrons. For large wave packets with $\sigma_0 \gg \sigma_L$ and with a sufficiently low divergence rate $\sigma'_0 \ll \lambda_C/\sigma_0$, the condition (34) turns into

$$\sqrt{(2n + |l| + 1)} \ll \frac{\sigma_L}{\lambda_C} \frac{\sigma_L}{\sigma_0}. \quad (35)$$

From here it follows that for wave packets with $\sigma_0/\sigma_L \geq \sigma_L/\lambda_C$, even a Gaussian mode with $n = l = 0$ is relativistic. For a field strength of the order of 1 T, this happens when $\sigma_0 \sim 1$ mm, which can also be decreased if the divergence rate σ'_0 in (34) is taken into account.

IV. CONNECTION BETWEEN NSLG_f AND NSLG_H STATES

Before considering NSLG_H states in detail, we should note that their explicit wave function was obtained from the continuity of the optical functions at the boundary (24). In reality, not only these functions, but also the wave function itself is continuous. This is not surprising, because electron states in free space and inside the solenoid are defined by the ansatz of the same general form (4).

We also need to make a special note about the energies of the NSLG_f and NSLG_H states. Generally, the quantities given by Eqs. (15) and (30) are not equal to each

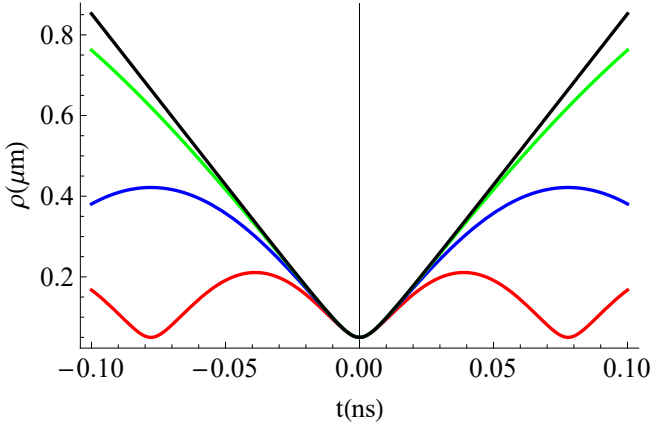


Figure 6: R.m.s. radius of an NSLG_H wave packet tends to $\rho_f(t)$ as the magnetic field decreases. NSLG_H packet r.m.s. radii are shown for: $H = 0.5$ T (in red), $H = 0.25$ (in blue), $H = 0.1$ T (in green); The NSLG_f electron r.m.s. radius $\rho_f(t)$ is indicated with the black line. The following parameters are used: $t_g = t_0 = 0$, $\rho_0 = \rho_w = 50$ nm, $\rho'_0 = \rho'_w = 0$, $n = 0$, and $l = 3$.

other, i.e. the energy is discontinuous at the boundary. This is a result of the energy dispersion, as the continuity of the average kinetic momentum $\langle \hat{p} \rangle$ does not provide that of $\langle E \rangle \sim \langle \hat{p}^2 \rangle \neq \langle \hat{p} \rangle^2$.

A. Vanishing magnetic field

One of the advantages of the NSLG_H states compared to the Landau ones is, they smoothly transform into free twisted electron wave packets in the vanishing magnetic field limit. To confirm this, we can find the limit of $\sigma(t), \Phi_G(t)$ as $H \rightarrow 0$ ($\sigma_L \rightarrow \infty$), see Appendix C for rigorous derivation. In Fig. 6, we show how NSLG_H dispersion transforms into that of the NSLG_f as the magnetic field goes to zero.

In contrast, the Landau states dispersion diverges in the vanishing magnetic field limit, and the wave functions become delocalized.

B. Off-axis injection

In a real-life setup, the propagation axis of a twisted electron wave packet cannot be perfectly aligned with the magnetic field direction. Such a misalignment can be caused by a shift of the electron source or slight inhomogeneities of the magnetic field inside the solenoid. In this section, we account for this inaccuracy by considering a twisted electron that enters the lens at a small angle α with respect to the z -axis, as shown in Fig. 7.

Imagine that by the time t_0 a free electron reaches the lens boundary at z_0 , the propagation axis of the electron is shifted by the angle α with respect to the z -axis aligned

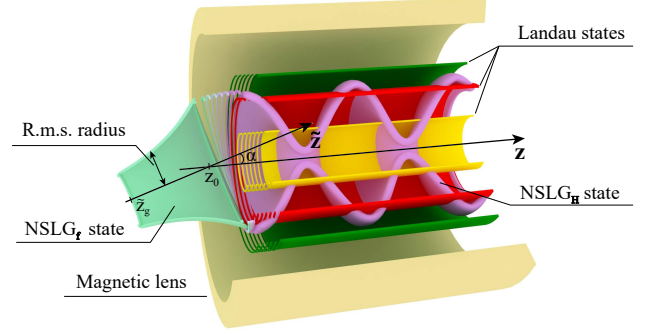


Figure 7: Free twisted electron entering a magnetic lens at a small angle α with respect to the field direction.

with the field. The wave function of the corresponding state is given by

$$\tilde{\Psi}_{nl}(\mathbf{r}, t) = \Psi_{nl}(\tilde{\mathbf{r}}, t) = \Psi_{nl}(\tilde{\rho}, t)\Psi_{\parallel}(\tilde{z}, t), \quad (36)$$

where the tilted coordinates

$$\begin{aligned} \tilde{z} &= z_0 - \rho \cos \varphi \sin \alpha + (z - z_0) \cos \alpha, \\ \tilde{\rho} &= \sqrt{(\rho \cos \varphi \cos \alpha + (z - z_0) \sin \alpha)^2 + \rho^2 \sin^2 \alpha}, \\ \tilde{\varphi} &= \arctan \left(\frac{\sin \varphi}{\cos \varphi \cos \alpha + \frac{z - z_0}{\rho} \sin \alpha} \right) \end{aligned} \quad (37)$$

are obtained by a rotation around the axis indicated by $\varphi = \pi/2$. The rotational symmetry of the problem enables an arbitrary choice of the rotation axis in the transverse plane without any influence on the results. The transverse and longitudinal parts of the wave function in Eq. (36) are given by Eqs. (4) and (3), respectively.

Let us now decompose the rotated wave function in terms of the electron states propagating along the z -axis:

$$\begin{aligned} \tilde{\Psi}_{nl}(\mathbf{r}, t) &= \sum_{n', l'} \int_{-\infty}^{\infty} \frac{dp'_z}{2\pi} c_{n'n'l'}(p'_z) \Psi_{n'l'}(\rho, t) \times \\ &g(p'_z) \exp \left(ip'_z z - i \frac{p'^2_z}{2m} t \right). \end{aligned} \quad (38)$$

Here, the decomposition coefficients are

$$\begin{aligned} c_{n'n'l'}(p'_z) &= \int d^2 \rho dz \Psi_{n'l'}^*(\rho, t) \Psi_{nl}(\tilde{\rho}, t) \times \\ &\int_{-\infty}^{\infty} \frac{dp_z}{2\pi} \exp \left(-ip'_z z + i \frac{p_z^2}{2m} t \right) \frac{g(p_z)}{g(p'_z)} \exp \left(ip_z \tilde{z} - i \frac{p_z^2}{2m} t \right). \end{aligned} \quad (39)$$

We are interested in the off-axis corrections to the electron state in the vicinity of the lens boundary. Therefore, we evaluate $\tilde{\Psi}_{nl}(\mathbf{r}, t)$ at $z = z_0$ and $t = t_0$ in Eq. (38).

In the first non-vanishing order in α and for $z = z_0$, Eqs. (37) are simplified to

$$\begin{aligned}\tilde{\rho} &= \rho + o(\alpha^2), \\ \tilde{\varphi} &= \varphi + o(\alpha^2), \\ \tilde{z} &= z - \alpha\rho \cos \varphi + o(\alpha^2),\end{aligned}\quad (40)$$

and the coefficients (39) take the form

$$c_{nn'l'l'}(p'_z) = \int \Psi_{n'l'}^*(\boldsymbol{\rho}, t) \Psi_{nl}(\boldsymbol{\rho}, t) \exp(-i\alpha p'_z \rho \cos \varphi) d^2\rho. \quad (41)$$

The integral over the transverse plane can be evaluated using Eq. (7.422) in [48] (there is, however, a misprint $m \leftrightarrow n$ in the book). The absolute value of the coefficients is

$$\begin{aligned}|c_{nn'l'l'}(p'_z) &= \delta_{n,n'} \delta_{l,l'} + \\ &\frac{\alpha p'_z \sigma(t_0)}{4\pi} \delta_{|l'|, |l|-1} \left[\delta_{n',n} \sqrt{n+|l|} + \delta_{n',n+1} \sqrt{n+1} \right] \\ &+ \frac{\alpha p'_z \sigma(t_0)}{4\pi} \delta_{|l'|, |l|+1} \left[\delta_{n',n} \sqrt{n+|l|+1} + \delta_{n',n-1} \sqrt{n} \right].\end{aligned}\quad (42)$$

If the longitudinal wave functions have a sufficiently narrow distribution in coordinate and momentum spaces simultaneously, we can evaluate the decomposition coefficients in a different manner. First, we can approximate the integrals over the longitudinal momentum by evaluating the integrand at the mean value $p_z = \langle p_z \rangle$. Then, Eq. (38) becomes

$$\Psi_{nl}(\tilde{\boldsymbol{\rho}}, t) \exp(-i\alpha \langle p_z \rangle \rho \cos \varphi) = \sum_{n',l'} c_{nn'l'l'}(\langle p_z \rangle) \Psi_{n'l'}(\boldsymbol{\rho}, t). \quad (43)$$

The expression (43), as compared to Eq. (38), does not contain the longitudinal wave function, whose entire contribution is accounted for by the average momentum $\langle p_z \rangle$. Proceeding in the same manner, we get

$$\begin{aligned}|c_{nn'l'l'}| &= \delta_{n,n'} \delta_{l,l'} + \\ &\frac{\alpha \langle p_z \rangle \sigma(t_0)}{4\pi} \delta_{|l'|, |l|-1} \left[\delta_{n',n} \sqrt{n+|l|} + \delta_{n',n+1} \sqrt{n+1} \right] \\ &+ \frac{\alpha \langle p_z \rangle \sigma(t_0)}{4\pi} \delta_{|l'|, |l|+1} \left[\delta_{n',n} \sqrt{n+|l|+1} + \delta_{n',n-1} \sqrt{n} \right].\end{aligned}\quad (44)$$

From Eq. (44), we see that the actual dimensionless parameter defining the magnitude of the coefficients is $\alpha \langle p_z \rangle \sigma(t_0)$. In real life, the value of $\sigma(t_0)$ is of the order of several μm or less. Provided that currently $n \sim 1$, $l \lesssim 10^4$, even for 10 GeV-electrons with $\langle p_z \rangle \sim 10^{-3} \mu\text{m}^{-1}$, we obtain $|c_{nn'l'l'}| \lesssim 10^{-2} \alpha$. This means that the off-axis corrections are negligible for any feasible experimental scenario.

V. CONNECTION BETWEEN NSLG STATES IN SOLENOID AND LANDAU STATES

A. Landau states as a special case of NSLG states

Although the Landau states (20) are represented by stationary wave functions, they also have the form (4). Moreover, both NSLG_H and Landau states are solutions of the Schrödinger equation (1) with the same Hamiltonian (16), which leads to the same system of optical equations (23). Here, the question arises: how these two sets of states are linked?

To answer this question, one may look for a solution of the system (23) corresponding to the stationary Landau states. Such a solution exists for the unique choice of the initial conditions:

$$\sigma_0 = \sigma_L, \quad \sigma'_0 = 0. \quad (45)$$

This means that the Landau states are but a special case of the NSLG_H ones forming when a free twisted electron with a specific size and zero divergence rate crosses the boundary. Otherwise, an electron inside the solenoid is described by general NSLG_H states rather than the Landau ones.

To characterize the deviation of the NSLG_H states from the Landau ones, we introduce two dimensionless parameters

$$\xi_1 = \frac{\sigma_L}{\sigma_0}, \quad \xi_2 = \frac{|\sigma'_0| \sigma_L}{\lambda_C}. \quad (46)$$

From Eq. (45), it follows that for the Landau states $\xi_1 = 1$, $\xi_2 = 0$. The more these parameters differ from 1 and 0, respectively, the more distinguishable the NSLG_H and the Landau states are. This effect manifests itself most clearly in growing amplitude of the r.m.s. radius oscillations and its period-averaged value.

B. Comparison of sizes of NSLG_H and Landau states

To characterize the size of an NSLG_H electron, we use the stationary radius ρ_{st} given by Eq. (28). Naively, it seems that this value should be equal to or at least close to ρ_L [29, 32, 33]. However, this is generally not true. In terms of the parameters (46), ρ_{st} is expressed as

$$\rho_{\text{st}} = \rho_L \left[\frac{\xi_1^2 + \xi_1^{-2}}{2} + \frac{\xi_2^2}{2} \right]^{1/2} \geq \rho_L. \quad (47)$$

From this expression, it is clear that for $\xi_1 \gg 1$, $\xi_1 \ll 1$, or $\xi_2 \gg 1$, the relation $\rho_{\text{st}}^2 \gg \rho_L^2$ holds. In contrast, for the initial conditions (45), when the electron in the field is indeed in the Landau state, the minimum value $\rho_{\text{st}} = \rho_L$ is reached. This illustrates that boundary conditions significantly affect the electron states inside the lens.

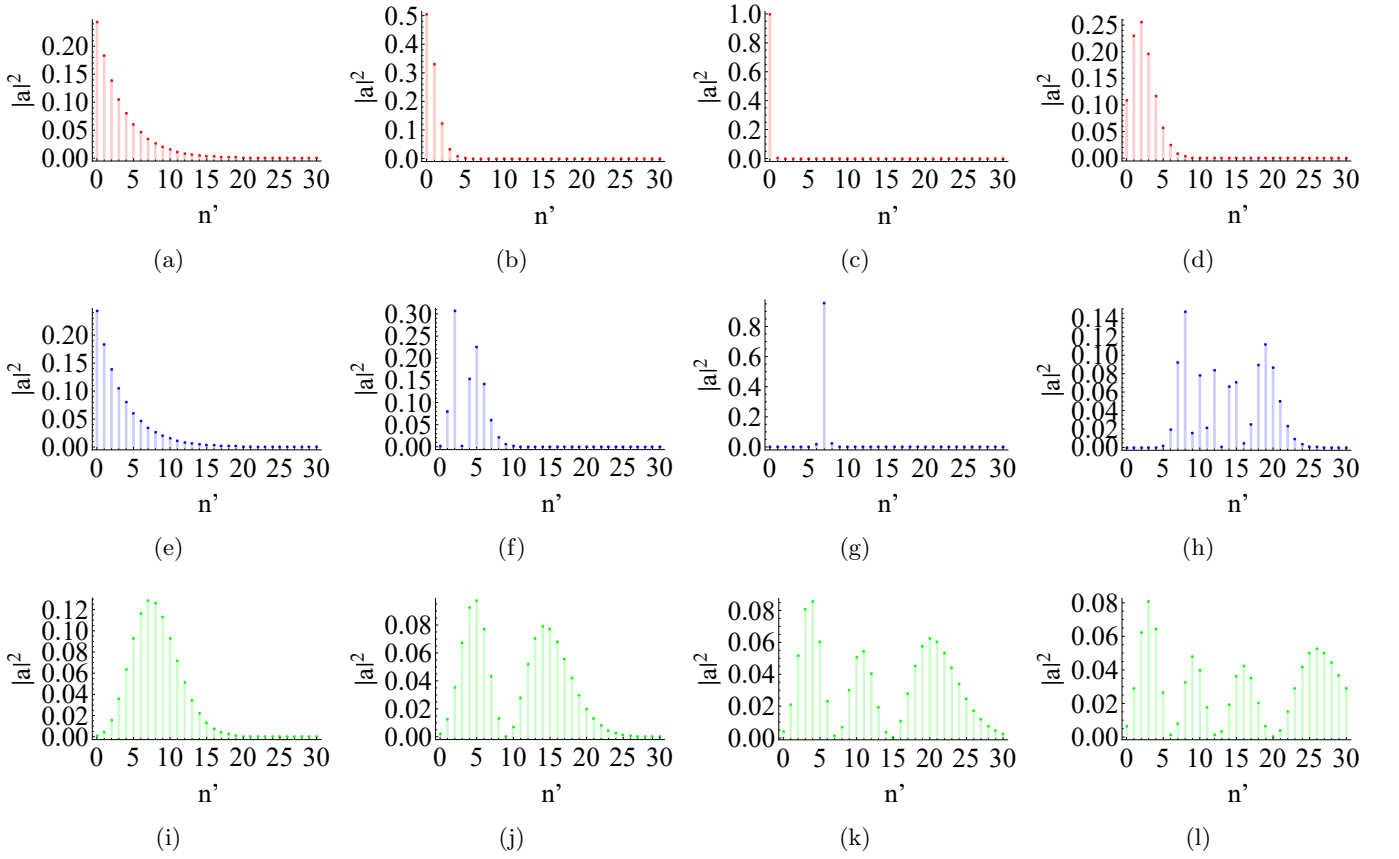


Figure 8: Probability coefficients $|a_{nn'l}|^2$ for an NSLG state with the quantum numbers n, l decomposed into a superposition of the Landau states with the quantum numbers n', l . $\rho_0 = 100$ nm, $\rho'_0 = 0$, $B = 1.9$ T. Top panel (in red): (a) $n = 0, l = 0$, (b) $n = 0, l = 7$, (c) $n = 0, l = 13$, (d) $n = 0, l = 25$; middle panel (in blue): (e) $n = 0, l = 0$, (f) $n = 3, l = 0$, (g) $n = 7, l = 0$, (h) $n = 12, l = 0$; bottom panel (in green): (i) $n = 0, l = 35$, (j) $n = 1, l = 35$, (k) $n = 2, l = 35$, (l) $n = 3, l = 35$.

The conditions imposed on the parameters $\xi_{1,2}$ for the NSLG_H state to be close to a Landau one are very specific. Unless an experimenter is intended to obtain a Landau state, an NSLG_H state is almost certainly generated. For example, in the experiment of Schattschneider et al. [17], the parameters of the setup $n = 0$, $|l| = 1$, $\sigma_0 = 4.77 \times 10^{-2} \mu\text{m}$, and $\sigma'_0 = -3.1 \times 10^{-4}$ lead to $\xi_1 = 0.76$ and $\xi_2 = 29.21 \gg 1$. For these parameters, we find $\rho_{\text{st}} = 20.7\rho_L \gg \rho_L$, which again supports our idea that NSLG_H states were observed in the work [17].

C. Decomposition of NSLG_H states in terms of Landau ones

Comparing the characteristic sizes of an NSLG_H and a Landau state, we qualitatively estimate the difference between the two states. For a more substantive investigation, we should decompose an NSLG_H state wave func-

tion in terms of the stationary Landau ones (20):

$$\Psi_{nl}(\boldsymbol{\rho}, t) = \sum_{n', l'} a_{nn'l} \delta_{l, l'} \Psi_{n'l'}^{(L)}(\boldsymbol{\rho}, t). \quad (48)$$

Since the evolution of both sides in Eq. (48) is governed by the same Hamiltonian, the decomposition coefficients do not depend on time. We present the explicit expression for $a_{nn'l}$ in the Appendix D. Note that the Kronecker delta reflects the OAM conservation.

As we have discussed in the previous section, $\rho_{\text{st}} = \rho_L$ only when NSLG_H and Landau states coincide. Indeed, from this equality, it follows that

$$a_{nn'l} = \delta_{n, n'}. \quad (49)$$

However, in experiment, it is impossible to precisely satisfy the initial conditions (45) to obtain a single Landau mode inside the solenoid.

Let us analyze what happens to the NSLG_H state inside the lens when its characteristic size and ρ_L with the same quantum numbers n, l are close, yet not equal:

$$\delta\zeta = \frac{\rho_{\text{st}} - \rho_L}{\rho_L} \ll 1. \quad (50)$$

This is true when the size of the incoming packet at the boundary slightly differs from ρ_L and the divergence rate is low. From Eq. (25), we know that in this situation, rather than being constant and equal to ρ_L , the r.m.s. radius inside the lens begins oscillating around a slightly larger value, ρ_{st} , with a small amplitude. The decomposition coefficients clearly indicate that for a small detuning, a few neighbouring Landau modes contribute to the NSLG_H state:

$$a_{nn'l} \propto (\delta\zeta)^{\frac{|n'-n|}{2}}. \quad (51)$$

Interference of these different states results in the r.m.s. radius oscillations and a change in the period-averaged size.

An intricate picture arises when the state inside the solenoid significantly differs from any of the Landau states, i.e. $\xi_1 \gg 1$, or $\xi_1 \ll 1$, or $\xi_2 \gg 1$. In this case, the NSLG_H state is a superposition of numerous Landau ones. The coefficients form wide, oscillating distributions as functions of the radial quantum number of the Landau states n' .

Examples of the probability coefficients $|a_{nn'l}|^2$ for the possible scenarios are presented in Fig. 8. We choose $\rho_0 = 100$ nm, $\rho'_0 = 0$, and $H = 1.9$ T, for which $\sigma_L \approx 26$ nm.

In Figs. 8a — 8d (top panel, in red), we study the distribution of $|a_{nn'l}|^2$ for different values of l while keeping $n = 0$. In Fig. 8a, $l = 0$ and $\rho_L \approx 26$ nm, so the NSLG_H state is wider than the Landau one with corresponding quantum numbers. As a consequence, higher-order Landau modes appear in the decomposition. Then, with increasing OAM (Figs. 8b, 8c), ρ_L gets closer to ρ_0 , making the decomposition similar to $\delta_{n,n'}$. With the further increase of OAM shown in Fig. 8d, ρ_L becomes larger than ρ_0 , and, once again, higher-order Landau modes appear. In this case, all the Landau states have a larger size than the NSLG_H state at the boundary. However, their destructive interference results in size suppression (see. (D4)).

In Figs. 8e — 8h (middle panel, in blue), we set $l = 0$ and investigate how n affects the probability coefficients. In general, the distribution of $|a_{nn'l}|^2$ is similar to that in Figs. 8a — 8d in the following sense. With increasing n , ρ_L grows, and for $n = 7$, when $\rho_L \approx \rho_0$, a δ -like peak emerges in Fig. 8g in accordance with Eq. (51). With a further increase in n , this peak vanishes, leading to numerous Landau states in Fig. 8h.

Figs. 8i — 8l (bottom panel, in green) demonstrate another peculiarity of the probability coefficients distribution. Namely, for sufficiently wide distributions, the number of peaks equals $n + 1$. We suppose this might be connected to the number of rings of the NSLG_H state; however, the true nature of this phenomenon is still unclear to us.

VI. EMITTANCE

A. Emittance and the Schrödinger uncertainty relation

Classical accelerator physics mainly focuses on particle beams, described by distribution functions in phase space. At any moment of time (or any distance z along the direction of beam propagation), every particle in a beam is a point in this space. In systems with axial symmetry, dynamics in two transverse directions are independent and indistinguishable when the beam has no classical vorticity [49]. This allows monitoring only one transverse coordinate $x(s)$ and the corresponding velocity projection $x'(s)$, which form two-dimensional trace space $(x(s), x'(s))$. Here, s is a variable parametrizing the particle motion, e.g., time or longitudinal coordinate.

Emittance is one of the essential measured parameters describing a beam. Depending on the problem, it can be defined in different ways; but the most common definitions are the trace space area and the r.m.s. emittance [50, 51]. The latter is

$$\epsilon_x = \sqrt{\langle x^2 \rangle \langle x'^2 \rangle - \langle xx' \rangle^2}, \quad (52)$$

with averaging performed over the beam distribution function, and $\langle x \rangle = \langle x' \rangle = 0$ is assumed. Due to the Liouville's theorem, the phase space volume (or the trace space area) is conserved, but such a definition of emittance does not distinguish between different particle distributions in beams with the same area. Vice versa, the r.m.s. emittance is not generally constant in time, however, it is sensitive to beam distribution [50]. One of the reasons why r.m.s. emittance depends on time is beam mismatch, which leads to r.m.s. radius oscillations [50, 52].

We will now draw analogies between quantum mechanics and classical accelerator physics. While in the latter, particles are points in the phase space, in quantum theory, a single particle packet is smeared in the coordinate and momentum spaces. In quantum mechanics, a quantity similar to that given by Eq. (52) arises from the Schrödinger uncertainty relation [29, 53]

$$(\Delta\hat{a})^2(\Delta\hat{b})^2 \geq \left(\frac{1}{2} \langle \{\hat{a}, \hat{b}\} \rangle - \langle \hat{a} \rangle \langle \hat{b} \rangle \right)^2 + \frac{1}{4} \left| \langle [\hat{a}, \hat{b}] \rangle \right|^2, \quad (53)$$

where \hat{a} and \hat{b} are Hermitian operators. A more illustrative form of this inequality is

$$(\Delta\hat{a})^2(\Delta\hat{b})^2 - \left(\langle \hat{a}\hat{b} \rangle - \langle \hat{a} \rangle \langle \hat{b} \rangle \right) \left(\langle \hat{b}\hat{a} \rangle - \langle \hat{b} \rangle \langle \hat{a} \rangle \right) \geq 0. \quad (54)$$

Note that for $\langle \hat{a} \rangle = \langle \hat{b} \rangle = 0$, the l.h.s. of Eq. (54) has the same form as the r.h.s. of Eq. (52). Thus, when \hat{a} and \hat{b} are the transverse coordinate and velocity operators, respectively, it is natural to call the l.h.s. of Eq. (54) the *quantum r.m.s. emittance*, see [29] for more detail. This

way, we see that the r.m.s. emittance definition can be naturally extended to quantum mechanics.

In classical physics, the smaller the r.m.s. emittance is, the less disordered is the beam. In quantum mechanics, the r.m.s. emittance acquires a new meaning: it reflects *non-classicality* of the state. When the emittance is vanishing, the position-momentum uncertainty is minimal, similar to a classical particle, whose momentum and coordinate can both be measured with minimal error. In contrast, the larger the quantum emittance is, the more noticeable the quantum nature of the particle becomes.

B. Quantum emittance of Laguerre-Gaussian wave packets

We now derive the quantum r.m.s. emittance of the NSLG_f and NSLG_H states:

$$\epsilon_i = \sqrt{\langle x_i^2 \rangle \langle \hat{v}_i^2 \rangle - \langle x_i \hat{v}_i \rangle \langle \hat{v}_i x_i \rangle} = \frac{1}{2} \sqrt{\langle \rho^2 \rangle \langle \hat{v}^2 \rangle - \langle \rho \cdot \hat{v} \rangle \langle \hat{v} \cdot \rho \rangle} \equiv \frac{\epsilon}{2}. \quad (55)$$

Here, i enumerates the two transverse axes. The second equality stems from the axial symmetry, and $\hat{v} = -i\lambda_C(\nabla - ie\mathbf{A})$ is the kinetic velocity operator. In Eq. (55), the averaging is performed over the NSLG_f or the NSLG_H states to obtain the corresponding emittance.

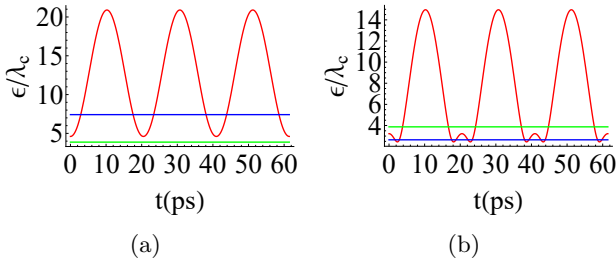


Figure 9: Emittances of the NSLG_H (in red), the Landau (in blue), and the NSLG_f (in green) states. $B = 1.9$ T, $n = 0$, $\sigma_0 = 25$ nm, $\sigma' = 0$. (a) $l = 3$, (b) $l = -3$.

Using

$$\langle \rho \cdot \hat{v} \rangle = \langle \hat{v} \cdot \rho \rangle^* = \frac{1}{2} \partial_t \langle \rho^2 \rangle(t) + i\lambda_C \quad (56)$$

the r.m.s. emittance can be expressed through the r.m.s. radius, its derivative, and the average energy as

$$\epsilon = \sqrt{2\lambda_C \langle \rho^2 \rangle(t) \langle E \rangle - \frac{1}{4} [\partial_t \langle \rho^2 \rangle(t)]^2 - \lambda_C^2}. \quad (57)$$

Let us first focus on the NSLG_f state. By substituting explicit expressions for the wave packet parameters from Eqs. (13) and (15) into Eq. (57), we get

$$\epsilon_f = \lambda_C \sqrt{(2n + |l| + 1)^2 - 1}. \quad (58)$$

The r.m.s. emittance of a free particle is constant in time and minimal for the Gaussian electron state when $n = l = 0$. Notice that this state minimizes the Schrödinger uncertainty, not the Heisenberg one. We should note this state is a special case of the coherent states of a free particle discussed in [54]. For $n, |l| \sim 1$, the quantum emittance of an NSLG_f state is of the order of λ_C , i.e. the particle stays relatively “classical”. For large quantum numbers, the emittance grows linearly, and the quantum nature of the particle becomes more pronounced.

Similarly, using NSLG_H optical functions and energy discussed in II E, we obtain the r.m.s. emittance of an NSLG electron inside the solenoid:

$$\epsilon_H(t) = \lambda_C \sqrt{\frac{\epsilon_f^2}{\lambda_C^2} + \left[(2n + |l| + 1) \frac{\sigma^2(t)}{\sigma_L^2} + l \right]^2 - l^2}. \quad (59)$$

The r.m.s. emittance of an NSLG_H state is defined by the dispersion $\sigma(t)$. The time dependence stems from the mismatch at the boundary ($\sigma_0 \neq \sigma_L$ and/or $\sigma'_0 \neq 0$), which causes the r.m.s. radius and, hence, the r.m.s. emittance oscillations.

From Eq. (59), the r.m.s. emittance of the Landau state can be easily obtained by setting $\sigma(t) = \sigma_L$:

$$\epsilon_L = \lambda_C \sqrt{\frac{\epsilon_f^2}{\lambda_C^2} + (2n + |l| + l + 1)^2 - l^2}. \quad (60)$$

One can notice that the r.m.s. emittance is discontinuous at the boundary. This can be seen from Eq. (57): the dispersion and its derivative are continuous, while the average energy is not, as we discussed in the beginning of Sec. IV.

The time dependence of the NSLG_H emittance is shown in Fig. 9. Unlike the r.m.s. radius, it is sensitive to the OAM sign. For $l < 0$ (Fig. 9a), r.m.s. emittance has additional local maxima, in contrast to the case when the OAM and the magnetic field are aligned (Fig. 9b).

Following the idea that smaller quantum r.m.s. emittance corresponds to a “more classical” particle behavior, we will analyze the regime when $\epsilon_H(t) < \epsilon_f$. For $n, |l| \sim 1$, it means that $\epsilon_H \lesssim 1$. Fig. 9 shows that for some parameters of the wave packet, there are time intervals when this condition is satisfied. From Eq. (59), this is possible only for $l < 0$. Moreover, the following relation has to be fulfilled:

$$\frac{2n + |l| + 1}{4|l|} + \frac{|l|}{2n + |l| + 1} < \frac{\sigma_{st}^2}{\sigma_L^2} < \frac{2|l|}{2n + |l| + 1}. \quad (61)$$

Note that for n or $l \gg 1$, NSLG_H emittance greatly exceeds λ_C when these inequalities are violated.

Therefore, the emittance of an NSLG electron can be locally decreased if the electron is placed in the field. However, if we consider a finite-length solenoid, the emittance changes abruptly at both boundaries, and when the particle leaves the solenoid, the emittance is exactly the same as it was at the entrance. Thus, our findings open ways for altering the r.m.s. emittance of an electron with magnetic lenses.

VII. RESULTS AND DISCUSSION

We have analyzed the properties of nonstationary Laguerre-Gaussian (NSLG) states, which, unlike the Landau states, fully capture vortex electron dynamics both at the vacuum-solenoid boundary and inside the magnetic field. Wave functions of an electron in free space and in the magnetic field belong to the same class of functions, which enables a smooth transition between single-mode states with the same quantum numbers.

The vector potential of the magnetic field was chosen in the symmetric gauge, which has led us to the Laguerre-Gaussian states. However, an alternative choice of the vector potential gauge would result in a different family of states, such as Hermite-Gaussian states. Which gauge to use is determined by the initial state of an electron in free space and, therefore, by the boundary conditions.

The decomposition of the NSLG states in a solenoid into the conventional basis of the Landau states was performed. A wave packet slightly mismatched with a Landau state at the boundary propagates through the magnetic lens as a superposition of a few Landau states with *the same* OAM and neighbouring radial quantum numbers. In other cases the electron further propagates in the field as a complex superposition of Landau states with the OAM of the initial state but significantly different radial quantum numbers.

We have considered a twisted electron entering the solenoid at a small angle α to the field direction. For any sensible values of the electron energy and momentum, the condition $\alpha \ll 1$ rad is sufficient to neglect any corrections to a single NSLG state in a solenoid. Thus, the OAM of the quantum packet is robust against little deviations from the axial symmetry and small inhomogeneities of the field, which supports our previous findings [29].

Our calculations show that transversely relativistic and longitudinally nonrelativistic beams of twisted particles can be achieved in existing experimental setups. For instance, electrons with quantum numbers of the order of 10^3 , generated as NSLG states with a waist size of $1 \mu\text{m}$ and focused afterwards to 1 nm , become transversely relativistic. Such particles can be a curious object of study in accelerator physics, as their dynamics significantly differs from that of regular accelerator beams.

Finally, we have introduced the quantum analogue of beam emittance for a quantum wave packet and applied it to the NSLG state. This quantity explicitly measures the non-classicality of the state via the Schrödinger uncertainty relation, which is more general than the well-known Heisenberg inequality. The quantum emittance of an NSLG state grows linearly with n and l for large quantum numbers. In free space, for fundamental Gaussian mode ($n = l = 0$), the emittance vanishes, or, equivalently, the Schrödinger uncertainty relation turns into equality. This reflects the semiclassical character of the Gaussian state and the “quantumness” of the wave packets with large quantum numbers n and l . For an electron

inside the field, the emittance generally oscillates in time, and for negative OAM, it can be locally lower than the emittance of a free NSLG state that enters the lens.

VIII. CONCLUSION

Let us give a final wrap up. The Landau states play a paramount role in problems with magnetic fields. They serve as a convenient basis when studying motion of the electrons in condensed matter or radiation in the field. However, once particles are allowed to transfer between vacuum and the magnetic field region, be it free space or a crystal, the NSLG states appear as a more advantageous means for describing particle states. The nonstationary nature of the processes under study is imprinted into the time dependence of the NSLG wave functions, and continuity with the free-space states comes naturally. We hope that the next time the reader analyzes an issue of the electron injection into magnetic field, they take a moment to consider which fighter to choose.

ACKNOWLEDGEMENT

We are grateful to S. Baturin, A. Volotka, and D. Glazov for the fruitful discussions and criticism. The studies in Secs. II are supported by the Russian Science Foundation (Project No. 21-42-04412; <https://rscf.ru/en/project/21-42-04412/>). The studies in Sect. III are supported by the Ministry of Science and Higher Education of the Russian Federation (agreement No.075-15-2021-1349). The work on the quantum states (by D. Karlovets, G. Sizykh, and D. Grosman) in Sec.IV was supported by the Foundation for the Advancement of Theoretical Physics and Mathematics “BASIS”. The studies in Sec. V are supported by the Government of the Russian Federation through the ITMO Fellowship and Professorship Program. The studies in Sec.VI are supported by the Russian Science Foundation (Project No. 23-62-10026; <https://rscf.ru/en/project/23-62-10026/>).

Appendix A: Completeness of NSLG states

We can prove that the set of states (4) is complete the following way. Let us consider a moment of time $t = \mathcal{T}$ such that $\sigma(\mathcal{T}) = \sigma$ and $\sigma'(\mathcal{T}) = 0$. This corresponds to $R(\mathcal{T}) \rightarrow \infty$, and the wave function (4) takes the following form:

$$\Psi_{nl}(\boldsymbol{\rho}, \mathcal{T}) = \Psi^{(L)}(\rho, \varphi, t) \exp(-i\Phi_G(\mathcal{T}) + iE_L t). \quad (\text{A1})$$

Here, $\Psi^{(L)}(\rho, \varphi, t)$ are the wave functions of the Landau states in an effective magnetic field $H_{\text{eff}} = 2/(e_0\sigma^2)$, which are complete in $\mathcal{L}^2(\mathbb{R})$, and t is an arbitrary moment of time. Completeness of Hermite-Gaussian

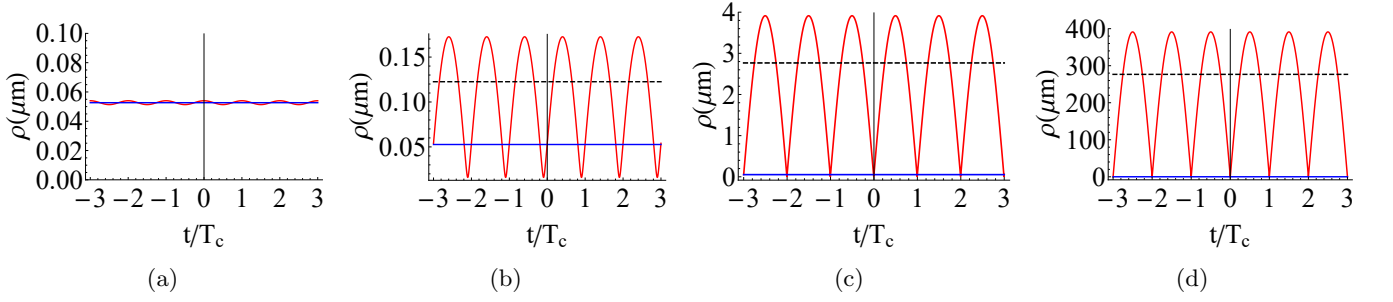


Figure 10: The NSLG_H packet r.m.s. radii (in red) for different ρ'_0 . The Landau radius ρ_L is in blue. Black dashed lines correspond to ρ_{st} given by Eq. (28). In each subfigure $H = 1.9$ T ($T_c \approx 0.02$ ns), $n = 0$, $l = 3$, $\rho_0 = 54$ nm. (a) $\rho'_0 = 0$, (b) $\rho'_0 = 4 \times 10^{-5}$, (c) $\rho'_0 = 10^{-3}$, (d) $\rho'_0 = 0.1$.

functions is proven in Theorem 11.4 in [55], which can be directly adopted to the Laguerre-Gaussian counterparts $\Psi^{(L)}(\rho, \varphi, t)$. From Eq. (A1), it is clear that if $c_{nl}(t)$ are the decomposition coefficients of some function of (ρ, t) into Landau states, then $\tilde{c}_{nl}(t) = c_{nl}(t) \exp(i\Phi_G(\mathcal{T}) - iE_L t)$ are the decomposition coefficients for the same function into NSLG states (4) evaluated at a time $t = \mathcal{T}$. Let us now decompose some function $F(\rho, t)$ into the wave functions (4) at an *arbitrary* moment of time. First, we consider another function $G(\rho, t) = \exp(i\hat{\mathcal{H}}(t - \mathcal{T}))F(\rho, t)$, where $\hat{\mathcal{H}}$ is the transverse part of the Hamiltonian of an electron in free space or in a magnetic field. The function $G(\rho, t)$ can be uniquely decomposed into Landau states and, hence, into NSLG states evaluated at a time $t = \mathcal{T}$:

$$G(\rho, t) = \exp(i\hat{\mathcal{H}}(t - \mathcal{T}))F(\rho, t) = \sum_{n,l} c_{nl}(t) \Psi^{(L)}(\rho, \varphi, t) = \sum_{n,l} \tilde{c}_{nl}(t) \Psi_{nl}(\rho, \mathcal{T}). \quad (\text{A2})$$

Acting on the l.h.s. and r.h.s. of Eq. (A2) with $\exp(-i\hat{\mathcal{H}}(t - \mathcal{T}))$, which is the evolution operator for the states (4), we obtain

$$F(\rho, t) = \sum_{n,l} \tilde{c}_{nl}(t) \Psi_{nl}(\rho, t), \quad (\text{A3})$$

which proves the completeness of the NSLG states.

Moreover, if the functions to be decomposed and the NSLG states satisfy the Schrödinger equation with the same Hamiltonian, and, thus, their time dependence is governed by the same evolution operator, the decomposition coefficients are independent of time. Indeed, consider the decomposition

$$\Psi(\rho, t) = \sum_{n,l} c_{nl}(t) \Psi_{nl}(\rho, t), \quad (\text{A4})$$

where $\Psi(\rho, t)$ and $\Psi_{nl}(\rho, t)$ satisfy the same Schrödinger equation. Since Eq. (A4) is valid for any moment of time, we also have the following decomposition:

$$\Psi(\rho, 0) = \sum_{n,l} c_{nl}(0) \Psi_{nl}(\rho, 0). \quad (\text{A5})$$

Acting on both sides of Eq. (A6) with the evolution operator, which does not affect the decomposition coefficients, we arrive at

$$\Psi(\rho, t) = \sum_{n,l} c_{nl}(0) \Psi_{nl}(\rho, t). \quad (\text{A6})$$

Now we recall that the set of the NSLG states is complete, and the choice of the decomposition coefficients is unique, meaning $c_{n,l}(t) = c_{n,l}(0)$, which, in turn, implies that the coefficients in this case do not depend on time.

Appendix B: Influence of divergence rate on oscillations

The initial divergence rate of the NSLG_H wave packet significantly influences its r.m.s. radius oscillations. The effect is depicted in Fig. 10. We choose the parameters as follows: $H = 1.9$ T, $n = 0$, $l = 3$, $\rho_0 = 25$ nm.

Fig. 10a serves as a reference with $\rho'_0 = 0$. In Fig. 10b, the divergence rate $\rho'_0 = 4 \times 10^{-5}$ such that the second and the third terms of σ_{st}^2 in Eq. (25) both contribute to its value. The nonzero divergence rate leads to a little shift in the initial phase of the oscillations θ and increase of their amplitude. Note that a change in the sign of ρ'_0 does not alter the amplitude and simply results in the phase shift with the opposite sign according to Eqs. (25). In Fig. 10c, the divergence rate is $\rho'_0 = 10^{-3}$. For such a high value of ρ'_0 , the initial phase of oscillations is negligible, and the amplitude is enhanced even more. In this regime, the magnitude grows proportionally to ρ'_0 , that is clear from the comparison of Figs. 10c and 10d.

Appendix C: Vanishing magnetic field limit of optical functions

Consider the dispersion of the NSLG_H state. Let us rewrite it by substituting the phase of oscillations θ :

$$\begin{aligned}\sigma^2(t) &= \sigma_{\text{st}}^2 + \sigma_{\text{st}}^2 \sqrt{1 - \frac{\sigma_{\text{L}}^4}{\sigma_{\text{st}}^4}} \sin(s(\sigma_0, \sigma'_0)\omega\tau - \theta) \\ &= \sigma_{\text{st}}^2 - (\sigma_{\text{st}}^2 - \sigma_0^2) \cos(\omega\tau) \\ &\quad + s(\sigma_0, \sigma'_0) \sin(\omega\tau) \sqrt{2\sigma_0^2\sigma_{\text{st}}^2 + \sigma_0^4 - \sigma_{\text{L}}^4},\end{aligned}\quad (\text{C1})$$

where $\tau = t - t_0$. In the vanishing magnetic field limit, when $H \rightarrow 0$ and $\sigma_{\text{L}} \rightarrow \infty$, the stationary dispersion can be simplified to

$$\sigma_{\text{st}} = \sigma_{\text{L}}^2 \left(\frac{1}{2\sigma_0^2} + \frac{\sigma_0'^2}{2\lambda_{\text{C}}^2} \right)^{1/2}. \quad (\text{C2})$$

Now we only keep the nonvanishing terms in Eq. (C1) in the limit $H \rightarrow 0$:

$$\sigma^2(t) \rightarrow \sigma_0^2 + 2\lambda_{\text{C}}^2\tau^2 \left(\frac{1}{2\sigma_0^2} + \frac{\sigma_0'^2}{2\lambda_{\text{C}}^2} \right) + \frac{2\sigma_0'\tau}{\sigma_0}. \quad (\text{C3})$$

Then we express σ_0 and σ_0' via the waist dispersion and the diffraction time as

$$\sigma_0 = \sigma_{\text{w}} \sqrt{1 + \frac{(t_0 - t_{\text{g}})^2}{\tau_{\text{d}}^2}}, \quad \sigma_0' = \frac{\sigma_{\text{w}}^2(t_0 - t_{\text{g}})}{\tau_{\text{d}}^2 \sqrt{1 + \frac{(t_0 - t_{\text{g}})^2}{\tau_{\text{d}}^2}}}. \quad (\text{C4})$$

Substituting Eq. (C4) into Eq. (C3) yields

$$\sigma(t) = \sigma_{\text{w}} \sqrt{1 + \frac{(t_0 - t_{\text{g}})^2}{\tau_{\text{d}}^2}}. \quad (\text{C5})$$

Smooth transformations of other optical functions follow from the system of optical equations (23) and transformation of the dispersion demonstrated above.

Appendix D: Explicit form of decomposition coefficients

The coefficients of the NSLG_H state decomposition into stationary Landau wave functions are given by the following integral:

$$\begin{aligned}a_{nn'l} &= |N_{nl}|^2 \int_0^\infty \frac{\rho^{2|l|}}{(\sigma_{\text{L}}\sigma(t))^{|l|+1}} L_n^{|l'|} \left[\frac{\rho^2}{\sigma_{\text{L}}^2} \right] L_n^{|l|} \left[\frac{\rho^2}{\sigma^2(t)} \right] \times \\ &\quad \exp \left[- \left(\frac{\rho^2}{2\sigma_{\text{L}}^2} + \frac{\rho^2}{2\sigma^2(t)} \right) + \right. \\ &\quad \left. i \frac{\rho^2}{2\lambda_{\text{C}}R(t)} - i\Phi_{\text{G}}(t) + iE_{\text{L}}(t - t_0) \right] d^2\rho.\end{aligned}\quad (\text{D1})$$

The coefficients are independent of time and can be evaluated at $t = t_0$ for simplicity, when $\sigma(t_0) = \sigma_0$, $R(t_0) = \sigma_0/\sigma_0'$ and $\Phi_{\text{G}}(t_0) = \Phi_0$.

The integral can be evaluated using Eq.(7.422) in [48] (there is, however, a misprint $m \leftrightarrow n$) and presented in the following form:

$$a_{nn'l} = (\zeta^2 - 1)^{(n'-n)/2} g(\zeta) e^{i\chi_{nn'}}. \quad (\text{D2})$$

Here $\zeta = \rho_{\text{st}}/\rho_{\text{L}}$,

$$\begin{aligned}g(\zeta) &= \frac{(n + n' + |l|)!}{\sqrt{n!n!(n + |l|)!(n' + |l|)!}} \frac{(-2)^n}{(\lambda + 1)^{(n+n'+|l|+1)/2}} \times \\ &\quad \left| {}_2F_1 \left[-n, -n - |l|; -n - n' - |l|; \frac{\zeta^2}{2} + \frac{1}{2} \right] \right|\end{aligned}\quad (\text{D3})$$

is an analytic function, and the phase

$$\begin{aligned}\chi_{nn'l} &= \Phi_0 + \left\{ \begin{array}{l} 0, \text{ if } {}_2F_1 \geq 0. \\ \pi, \text{ if } {}_2F_1 < 0. \end{array} \right\} + \\ &\quad \pi \times \left\{ \begin{array}{l} n, \text{ if } \xi_1 < 1 \\ n', \text{ if } \xi_1 > 1 \end{array} \right\} + (n - n') \arctan \frac{\xi_1 \xi_2}{1 - \xi_1^2} + \\ &\quad (n + n' + |l| + 1) \arctan \frac{\xi_1 \xi_2}{1 + \xi_1^2}.\end{aligned}\quad (\text{D4})$$

In the limit $\zeta^2 \rightarrow 1$

$$\begin{cases} g(\zeta) \propto 1, \text{ if } n' > n, \\ g(\zeta) \propto (\zeta^2 - 1)^{n-n'}, \text{ if } n > n', \end{cases}\quad (\text{D5})$$

which provides the following asymptotic for the decomposition coefficients:

$$a_{nn'l} \propto (\delta\zeta)^{\frac{|n'-n|}{2}}. \quad (\text{D6})$$

[1] Konstantin Yu. Bliokh, Yury P. Bliokh, Sergey Savel'ev, and Franco Nori. Semiclassical dynamics of electron

wave packet states with phase vortices. *Phys. Rev. Lett.*, 99:190404, Nov 2007.

- [2] Konstantin Y. Bliokh, Mark Dennis, and Franco Nori. Relativistic electron vortex beams: Angular momentum and spin-orbit interaction. *Phys. Rev. Lett.*, 107:174802, Oct 2011.
- [3] Konstantin Y. Bliokh, Peter Schattschneider, Jo Verbeeck, and Franco Nori. Electron Vortex Beams in a Magnetic Field: A New Twist on Landau Levels and Aharonov-Bohm States. *Phys. Rev. X*, 2:041011, Nov 2012.
- [4] Gregg M. Gallatin and Ben McMorran. Propagation of vortex electron wave functions in a magnetic field. *Phys. Rev. A*, 86:012701, Jul 2012.
- [5] Dmitry Karlovets. Electron with orbital angular momentum in a strong laser wave. *Phys. Rev. A*, 86:062102, Dec 2012.
- [6] Colin Greenshields, Robert L Stamps, and Sonja Franke-Arnold. Vacuum Faraday effect for electrons. *New Journal of Physics*, 14(10):103040, Oct 2012.
- [7] I. Ivanov, V. Serbo, and V. Zaytsev. Quantum calculation of the vavilov-cherenkov radiation by twisted electrons. *Phys. Rev. A*, 93:053825, May 2016.
- [8] Dmitry Karlovets. Relativistic vortex electrons: Paraxial versus nonparaxial regimes. *Phys. Rev. A*, 98:012137, Jul 2018.
- [9] A. Maiorova, S. Fritzsche, R. Müller, and A. Surzhykov. Elastic scattering of twisted electrons by diatomic molecules. *Phys. Rev. A*, 98:042701, Oct 2018.
- [10] Robert Ducharme, Irismar da Paz, and Armen Hayrapetyan. Fractional Angular Momenta, Gouy and Berry Phases in Relativistic Bateman-Hillion-Gaussian Beams of Electrons. *Phys. Rev. Lett.*, 126:134803, Apr 2021.
- [11] D. Karlovets and A. Pupasov-Maksimov. Nonlinear quantum effects in electromagnetic radiation of a vortex electron. *Phys. Rev. A*, 103:012214, Jan 2021.
- [12] Lei Shaohu, Bu Zhigang, Wang Weiqing, Shen Baifei, and Ji Liangliang. Generation of relativistic positrons carrying intrinsic orbital angular momentum. *Phys. Rev. D*, 104:076025, Oct 2021.
- [13] J. Verbeeck, H. Tian, and Peter Schattschneider. Production and application of electron vortex beams. *Nature Lett.*, 467:301–304, Sep 2010.
- [14] Benjamin J. McMorran, Amit Agrawal, Ian M. Anderson, Andrew A. Herzing, Henri J. Lezec, Jabez J. McClelland, and John Unguris. Electron vortex beams with high quanta of orbital angular momentum. *Science*, 331(6014):192–195, 2011.
- [15] Giulio Guzzinati, Peter Schattschneider, Konstantin Bliokh, Franco Nori, and Jo Verbeeck. Observation of the larmor and gouy rotations with electron vortex beams. *Phys. Rev. Lett.*, 110:093601, Mar 2013.
- [16] T. Petersen, D. Paganin, M. Weyland, T. Simula, S. Eastwood, and M. Morgan. Measurement of the gouy phase anomaly for electron waves. *Phys. Rev. A*, 88:043803, May 2013.
- [17] P. Schattschneider, Th. Schachinger, M. Stöger-Pollach, S. Löffler, Steiger-Thirsfeld A., Bliokh K., and F. Nori. Imaging the dynamics of free-electron Landau states. *Nature Comm.*, 5:4586, Aug 2014.
- [18] T. Schachinger, S. Löffler, Stöger-Pollach M., and P. Schattschneider. Peculiar rotation of electron vortex beams. *Ultramicroscopy*, 158:17–25, Nov 2015.
- [19] J.C. Idrobo and S.J. Pennycook. Vortex beams for atomic resolution dichroism. *Microscopy*, 60:295–300, Oct 2011.
- [20] Z. Mohammadi, C.P. Van Vlack, S. Hughes, J. Bornemann, and R. Gordon. Vortex electron energy loss spectroscopy for near-field mapping of magnetic plasmons. *Optics Express*, 20:15024–15034, 2012.
- [21] Vincenzo Grillo, Tyler Harvey, Federico Venturi, Jordan Pierce, Roberto Balboni, Frédéric Bouchard, Gian Gazzadi, Stefano Frabboni, Amir Tavabi, Zi-An Li, Rafal Dunin-Borkowski, Robert Boyd, Benjamin McMorran, and Ebrahim Karimi. Observation of nanoscale magnetic fields using twisted electron beams. *Nature Comm.*, 8:689, Sep 2017.
- [22] K.Y. Bliokh, I.P. Ivanov, G. Guzzinati, L. Clark, R. Van Boxem, A. Béché, R. Juchtmans, M.A. Alonso, P. Schattschneider, F. Nori, and J. Verbeeck. Theory and applications of free-electron vortex states. *Physics Reports*, 690:1–70, 2017. Theory and applications of free-electron vortex states.
- [23] M. Uchida and A. Tonomura. Generation of electron beams carrying orbital angular momentum. *Nature*, 464:737–739, Apr 2010.
- [24] P. Schattschneider, M. Stöger-Pollach, and J. Verbeeck. Novel vortex generator and mode converter for electron beams. *Phys. Rev. Lett.*, 109:084801, Aug 2012.
- [25] A. Tavabi, P. Rosi, A. Roncaglia, E. Rotunno, M. Beleggia, P.-H. Lu, G. Belsito, L. Pozzi, S. Frabboni, P. Tiemeijer, R. E. Dunin-Borkowski, and V. Grillo. Generation of electron vortex beams with over 1000 orbital angular momentum quanta using a tunable electrostatic spiral phase plate. *Appl. Phys. Lett.*, 121:073506, Aug 2022.
- [26] J. Verbeeck, P. Schattschneider, S. Lazar, M. Stöger-Pollach, S. Löffler, A. Steiger-Thirsfeld, and G. Van Tendeloo. Atomic scale electron vortices for nanoresearch. *Appl. Phys. Lett.*, 9:203109, Oct 2011.
- [27] V. Grillo, E. Karimi, G.C. Gazzadi, S. Frabboni, M.R. Dennis, and R.W. Boyd. Generation of nondiffracting electron bessel beams. *Phys. Rev. X*, 4:011013, Jan 2014.
- [28] Zou Liping, Zhang Pengming, and Alexander Silenko. General quantum-mechanical solution for twisted electrons in a uniform magnetic field. *Phys. Rev. A*, 103:L010201, Jan 2021.
- [29] Dmitry Karlovets. Vortex particles in axially symmetric fields and applications of the quantum Busch theorem. *New Journal of Physics*, 23(3):033048, mar 2021.
- [30] Abhijeet Melkani and S. J. van Enk. Electron vortex beams in nonuniform magnetic fields. *Phys. Rev. Research*, 3:033060, Jul 2021.
- [31] S. Baturin, D. Grosman, G. Sizykh, and D. Karlovets. Evolution of an accelerated charged vortex particle in an inhomogeneous magnetic lens. *Phys. Rev. A*, 106:042211, Oct 2022.
- [32] C.R. Greenshields, R.L. Stamps, S. Franke-Arnold, and S.M. Barnett. Is the angular momentum of an electron conserved in a uniform magnetic field? *Phys. Rev. Lett.*, 113:240404, Dec 2014.
- [33] C.R. Greenshields, S. Franke-Arnold, and R.L. Stamps. Parallel axis theorem for free-space electron wavefunctions. *New J. Phys.*, 17:093015, 2015.
- [34] L. D. Landau and E. M. Lifshitz. *Quantum Mechanics: Nonrelativistic Theory*. Butterworth-Heinemann, Burlington, Massachusetts, 1981.
- [35] G. K. Sizykh, A. D. Chaikovskaia, D. V. Grosman, I. I. Pavlov, and D. V. Karlovets. Transmission of vortex electrons through a solenoid. *arXiv:2306.13161 [quant-ph]*,

June 2023.

- [36] Dmitry Karlovets and Alexey Zhevlakov. Intrinsic multipole moments of non-gaussian wave packets. *Phys. Rev. A*, 99:022103, Feb 2019.
- [37] Dmitry Karlovets. Dynamical enhancement of nonparaxial effects in the electromagnetic field of a vortex electron. *Phys. Rev. A*, 99:043824, Apr 2019.
- [38] D. Landau. Diamagnetismus der metalle. *Z. Phys.*, 64:629–637, Sep 1930.
- [39] O. Ciftja. Detailed solution of the problem of landau states in a symmetric gauge. *European Journal of Physics*, 41(3):035404, Apr 2020.
- [40] I. Malkin and V. Manko. *Dynamic symmetry and coherent states of quantum systems*. Izdatel'stvo Nauka, Moscow, 1979.
- [41] D. Gitman V. Bagrov. *The Dirac equation and its solutions*. Berlin [a. o.] : de Gruyter, 2014.
- [42] N. V. Filina and S. S. Baturin. Unitary equivalence of twisted quantum states. *Phys. Rev. A*, 108(1):012219, 2023.
- [43] A.E. Siegman. *Lasers*. Mill Valley, 1986.
- [44] S. Feng and H.G. Winful. Physical origin of the gouy phase shift. *Optics Letters*, 26:485–487, Apr 2001.
- [45] V. Grillo, G. Gazzadi, E. Mafakheri, S. Frabboni, E. Karimi, and R. Boyd. Holographic generation of highly twisted electron beams. *Phys. Rev. Lett.*, 114:034801, Jan 2015.
- [46] E. Mafakheri, A. Tavabi, P.-H. Lu, R. Balboni, F. Venturi, C. Menozzi, G.C. Gazzadi, S. Frabboni, A. Sit, R. E. Dunin-Borkowski, E. Karimi, and V. Grillo. Realization of electron vortices with large orbital angular momentum using miniature holograms fabricated by electron beam lithography. *Appl. Phys. Lett.*, 110:093113, Mar 2017.
- [47] B. McMorrnan, A. Agrawal, P. Ercius, V. Grillo, A. Herzog, T. Harvey, M. Linck, and J. Pierce. Origins and demonstrations of electrons with orbital angular momentum. *Phil. Trans. R. Soc.*, 375:20150434, Feb 2017.
- [48] I.S. Gradshteyn and I.M. Ryzhik. *Table of Integrals, Series, and Products*. FizMatGiz, Moscow, 4 edition, 1964.
- [49] L. Groening, C. Xiao, and M. Chung. Particle beam eigenemittances, phase integral, vorticity, and rotations. *Phys. Rev. Accel. Beams*, 24:054201, May 2021.
- [50] M. Reiser. *Theory and Design of Charged Particle Beams*. Wiley, New York, 2008.
- [51] M. Migliorati, A. Bacci, C. Benedetti, E. Chiadroni, M. Ferrario, A. Mostacci, L. Palumbo, A. R. Rossi, L. Serafini, and P. Antici. Intrinsic normalized emittance growth in laser-driven electron accelerators. *Phys. Rev. ST Accel. Beams*, 16:011302, Jan 2013.
- [52] R.J. Noble. Beam mismatch and emittance oscillations in magnetic transport lines. *Proceedings of the 1989 IEEE Particle Accelerator Conference*, pages 1067 – 1069, 1989.
- [53] E. Schrödinger. *Zum Heisenbergschen Unschärfepinzip*. Abhandlungen der Preussischen Akademie der Wissenschaften, Physikisch-Mathematische Klasse. Akademie der Wissenschaften, 1930.
- [54] V G Bagrov, D M Gitman, and A S Pereira. Coherent and semiclassical states of a free particle. *Physics-Uspekhi*, 57(9):891, sep 2014.
- [55] Brian C Hall. *Quantum theory for mathematicians*. Springer, 2013.